Crystal Structure and Enzyme Kinetics of the (*S*)-Specific 1-Phenylethanol Dehydrogenase of the Denitrifying Bacterium Strain EbN1[†,‡]

H. Wolfgang Höffken,[*,#] Minh Duong,[§] Thomas Friedrich,[||] Michael Breuer,[||] Bernhard Hauer,[||] Richard Reinhardt,[⊥] Ralf Rabus,[▽] and Johann Heider[§]

BASF AG, Physical Chemistry and Informatics, Fine Chemicals and Biocatalysis Research, 67056 Ludwigshafen, Germany, University Freiburg, Institute for Biology II, Microbiology, Schänzlestrasse 1, 79104 Freiburg, Germany, Max Planck Institute for Molecular Genetics, Ihnestrasse 73, 14195 Berlin, Germany, and Max Planck Institute for Marine Microbiology, Celsiusstrasse 1, 28359 Bremen, Germany

Received August 11, 2005; Revised Manuscript Received November 4, 2005

ABSTRACT: (*S*)-1-Phenylethanol dehydrogenase (PED) from the denitrifying bacterium strain EbN1 catalyzes the NAD^+-dependent, stereospecific oxidation of (*S*)-1-phenylethanol to acetophenone and the biotechnologically interesting reverse reaction. This novel enzyme belongs to the short-chain alcohol dehydrogenase/aldehyde reductase family. The coding gene (*ped*) was heterologously expressed in *Escherichia coli* and the purified protein was crystallized. The X-ray structures of the apo-form and the NAD^+-bound form were solved at a resolution of 2.1 and 2.4 Å, respectively, revealing that the enzyme is a tetramer with two types of hydrophobic dimerization interfaces, similar to β-oxoacyl-[acyl carrier protein] reductase (FabG) from *E. coli*. NAD^+-binding is associated with a conformational shift of the substrate binding loop of PED from a crystallographically unordered "open" to a more ordered "closed" form. Modeling the substrate acetophenone into the active site revealed the structural prerequisites for the strong enantioselectivity of the enzyme and for the catalytic mechanism. Studies on the steady-state kinetics of PED indicated a highly positive cooperativity of both catalytic directions with respect to the substrates. This is contrasted by the behavior of FabG. Moreover, PED exhibits extensive regulation on the enzyme level, being inhibited by elevated concentrations of substrates and products, as well as the wrong enantiomer of 1-phenylethanol. These regulatory properties of PED are consistent with the presence of a putative "transmission module" between the subunits. This module consists of the C-terminal loops of all four subunits, which form a special interconnected structural domain and mediate close contact of the subunits, and of a phenylalanine residue in each subunit that reaches out between substrate-binding loop and C-terminal domain of an adjacent subunit. These elements may transmit the substrate-induced conformational change of the substrate binding loop from one subunit to the others in the tetrameric complex and thus mediate the cooperative behavior of PED.

A number of secondary alcohol dehydrogenases specific for (*R*)- or (*S*)-enantiomers have been characterized to date from different sources. These enzymes are of biotechnological interest for the specific production of chiral alcohols from ketones (*1*). Most commercially available enzymes used in industry are broad-spectrum alcohol dehydrogenases, such as the enzymes from different yeast species or horse liver. Some enzymes are available for more specialized applications, for example, a hydroxysteroid dehydrogenase normally involved in cholesterol metabolism or a thermophilic alcohol dehydrogenase from *Thermoanaerobium brockii* (*2*). However, these enzymes often do not react well with a compound of interest or yield too much of the unwanted enantiomer. Therefore, screening efforts for new enantiomer-specific alcohol dehydrogenases with unusual substrate preferences represent an ongoing challenge. For example, an $NADP^+$-dependent (*R*)-1-phenylethanol dehydrogenase was purified from *Lactobacillus* species (*3*, *4*). This enzyme belongs to the short-chain family of alcohol dehydrogenases (*5*, *6*), whereas another purified NAD^+-dependent (*S*)-1-phenylethanol dehydrogenase (PED)[1] from *Rhodococcus erythropolis* belongs to the medium-chain, Zn^{2+}-containing alcohol dehydrogenases (*3*, *7*). The crystal structure of the (*R*)-specific alcohol dehydrogenase from *Lactobacillus brevis* was recently resolved, indicating that enantiospecificity of the NADP(H)-dependent enzyme was due to its hypothetical ternary structure (*8*). High-resolution structures of several other SDR enzymes (short-chain alcohol dehydrogenase/aldehyde reductase) have been reported (for overview see ref *9*). Further NAD^+-dependent (*S*)- and (*R*)-1-phenylethanol

[†] This work was supported by the Max Planck Gesellschaft (MPG), the Deutsche Forschungsgemeinschaft (DFG) and the BASF AG.

[‡] This work is dedicated to Franz Lingens on the occasion of his 80th birthday.

* To whom correspondence should be addressed. Tel: +49-621-60-49418. Fax: +49-621-60-4920440. E-mail: wolfgang.hoeffken@basf-ag.de.

[#] BASF AG, Physical Chemistry and Informatics.

[||] BASF AG, Fine Chemicals and Biocatalysis Research.

[§] University Freiburg, Institute for Biology II, Microbiology.

[⊥] Max Planck Institute for Molecular Genetics.

[▽] Max Planck Institute for Marine Microbiology.

[1] Abbreviations: PED, (*S*)-1-phenylethanol dehydrogenase.

10.1021/bi051596b CCC: $33.50 © 2006 American Chemical Society
Published on Web 12/08/2005

dehydrogenase activities were found in an *Arthrobacter* sp. grown aerobically with racemic 1-phenylethanol (*10*), in a *Corynebacterium* sp. (*11*) and in *Candida parapsilosis* (*12*), but these enzymes were not characterized in detail. Finally, an NAD^+-dependent (*S*)-enantiomer-specific 1-phenylethanol-dehydrogenase has recently been purified and characterized from the denitrifying bacterium strain EbN1 (*13*), and its coding gene was determined (*14*). Strain EbN1 forms (*S*)-1-phenylethanol by direct anaerobic oxidation of ethylbenzene by a novel molybdenum enzyme, ethylbenzene dehydrogenase (*15*). The bacterium belongs to a recently recognized phylogenetic cluster within *Betaproteobacteria*, the members of which are characterized by many novel anaerobic biochemical reactions (*16*−*18*). The recently determined genome sequence of strain EbN1 (*19*) contains genes for at least two further presumably enantioselective 1-phenylethanol dehydrogenases.

In the present study, the *ped* gene coding for PED was cloned from strain EbN1 and heterologously overexpressed in *Escherichia coli*. The enzyme was purified and crystallized, and its structure was determined. Moreover, kinetic studies revealed a highly cooperative catalysis of the enzyme and strong regulation of its activity. A possible link between the structural features and regulation of the enzyme is presented.

EXPERIMENTAL PROCEDURES

Cloning of ped Gene. Strain EbN1 was cultivated, and genomic DNA was prepared as described before (*14*, *16*). The *ped* gene was amplified by PCR using the oligonucleotide probes PED1_fw (5′-GGGAATTCCATATGACG-CAAAGACTGAAGG-3′) and PED1_rev (5′-CGCGGATC-CTCAGTGTCTCACCATACCGCC-3′). The reaction mixture contained 130 ng of each probe, 1 mM dATP, dCTP, dTTP, and dGTP, respectively, approximately 30 ng of a plasmid from a genomic library of strain EbN1 containing the *ped* gene (*14*), 5 μL of 10-times reaction buffer (Stratagene, La Jolla, CA), and 1 U of *Pfu*-DNA-polymerase (Stratagene) in a total volume of 50 μL. The mixture was heated for 5 min at 95 °C, and the gene was amplified by 30 cycles (annealing: 45 s at 55 °C, polymerization: 60 s at 72 °C, and melting: 45 s at 95 °C) plus a final extension at 72 °C for 10 min. PCR products were cleaved with *Nde*I and *Hind*III, ligated into appropriately prepared pJOE2702 vectors (*20*), and transformed into *E. coli* strain TG1 (*21*). Recombinant *E. coli* cells were grown in LB medium (*22*) and induced by the addition of 0.2% rhamnose. After 10 h of induction, the PED protein was highly overproduced in soluble form and purified as described below.

Enzyme Assays. The forward reaction of PED was measured with (*S*)-1-phenylethanol and NAD^+ as substrates, essentially as described by Kniemeyer and Heider (*13*). Tests were performed at 25 °C in a total volume of 250 μL of buffer (100 mM Tris-HCl, 2 mM $MgCl_2$, pH 7.8) containing 0.8−1.0 μg of recombinant enzyme in a microplate reader (μQuant; Bio-Tek Instruments, Bad Friedrichshall, Germany) with eight simultaneously started reactions per experiment. Reduction of NAD^+ after addition of (*S*)-1-phenylethanol was followed at 365 nm in triplicate assays. The concentrations of (*S*)-1-phenylethanol and NAD^+ were varied as indicated for the respective experiments. The reverse reaction of the enzyme was measured as acetophenone-dependent oxidation of NADH under the same conditions but with a 10-fold higher concentration of enzyme to compensate for the lower reaction rate. Evaluation of the data and curve fitting was performed with a standard program package (Prism4; GraphPad, San Diego, CA).

Molecular Mass Determination. The molecular mass of recombinant PED was determined by two independent methods. (i) The elution properties of the enzyme on a calibrated gel filtration column (Superdex 200 HR 10/30; Amersham Bioscience, Freiburg, Germany) were compared to those of standard proteins (ferritin, catalase, bovine serum albumin, ovalbumin). (ii) The migration behavior of the enzyme on native gels containing different polyacrylamide concentrations between 6 and 10% (w/v) was analyzed by Ferguson plot analysis and compared to that of bovine serum albumin oligomers (monomer − tetramer) and ovalbumin as recently described (*23*).

Purification of the Recombinant (S)-1-Phenylethanol Dehydrogenase from E. coli. For homogenization, 200 g of wet cell pellet were vigorously resuspended in 400 mL of a buffer containing 20 mM potassium phosphate (pH 7.4) and 10 μM NAD^+. The suspension was divided in 100 mL aliquots and homogenized on ice in a glass mill desintegrator (SCP-100-CMG; Innomed Konsult AB, Stockholm, Schweden). The material was filtered on G2 glas sinter filter. After washing of the beads with 20 mM potassium phosphate (pH 7.4) buffer, the volume was 870 mL. The homogenate was centrifuged for 20 min at 12 000 rpm (GSA-rotor, S-10233 centrifuge; Sorvall, Stockholm, Sweden). The supernatant (720 mL, pH 6.9) contained 26 000 U of enzyme activity and was used for chromatographic steps as follows (1 U equals 1 μmol min^{-1} mg^{-1}).

For a first ion exchange chromatography, a Q-sepharose column (fast flow, 5 cm diameter, 350 mL total volume; Pharmacia, Freiburg, Germany) was equilibrated with buffer A (20 mM potassium phosphate, 10 μM NAD^+, pH 6.8). The homogenate (720 mL) was applied at a flow rate of 8 mL/min. The column was then washed with 900 mL buffer A. The column was eluted with a linear gradient of buffer A to buffer B (buffer A with 0.75 M NaCl) over 1200 mL. However, virtually all the activity was found in the run-through and washing fractions. These fractions, which contained 20 000 U of enzyme activity (70%), were collected and combined in a total volume of 1460 mL.

The combined active fractions of the Q-sepharose chromatography were adjusted to 35% saturation with ammonium sulfate. Precipitated proteins (containing PED) were pelleted by centrifugation and redissolved in 500 mL of 20 mM potassium phosphate buffer pH 6.8 with the addition of 10 μM NAD^+ (final volume 600 mL). To this volume, 102 g of NaCl were added and the pH was adjusted to 6.0. After the sample was stirred for 20 min, the enzyme precipitated and was pelleted by centrifugation. This pellet could be stored at 4 °C for several days. It was redissolved in 1 L of water, and then 231 g of ammonium acetate (final concentration 3 M) was added. During this procedure, the pH was kept constant at 7.0.

A phenyl sepharose column (fast flow, 5 cm diameter, 300 mL volume; Pharmacia) was equilibrated with a solution of 3 M ammonium acetate and 10 μM NAD^+ (pH 7.0). The prepared protein solution in the same solvent (1180 mL) was

applied to the column at a flow rate of 10 mL/min. The column was then washed with 300 mL of the same buffer, and then it was developed by a linear gradient from 3 M ammonium acetate and 10 μM NAD^+ (pH 7.0) to water for 100 min at the same flow rate. After the column was washed with water for a further 50 min, another linear gradient from water to an aqueous solution of 10% (v/v) 2-propanol, 20 mM ammonium acetate, 10 μM NADH, pH 7.0 was applied for 30 min. Finally, the column was washed with 10% 2-propanol. During the last elution phase, two peaks containing active enzyme eluted (480 mL of peak I, containing 2000 U of enzyme activity and 1.15 g of protein, and 170 mL of peak II, containing 2300 U of enzyme activity and 0.88 g of protein).

Finally, a second ion exchange chromatography was performed on a Mono-Q column (Mono-Q, HR16/10, 20 mL; Pharmacia). The column was equilibrated with buffer C (20 mM MOPS buffer containing 10 μM NAD^+, pH 7.0) at a flow rate of 4 mL/min. The pooled fractions of peak II from the previous step were divided in half and applied on the column. Then the column was washed with 200 mL of buffer C, and a linear gradient from buffer C to buffer D (buffer C containing 0.5 M NaCl) was applied for 80 min. Some activity was found in the flow-through, but most of the enzyme bound to the column and was eluted as a single activity peak. The combined yield of activity was 1080 U (4.1% of the starting material). Active fractions were collected und used for crystallization. Enzyme activities measured during enzyme purification were significantly lower from those reported later because (*S*)-1-phenylethanol has initially been used in concentrations that exerted significant substrate inhibition. The purification scheme of PED is summarized in Supplementary Figure 1 and Supplementary Table 1 (Supporting Information).

Protein Crystallization and Data Collection. The crystals of PED were grown by the sitting drop method in a buffer containing 12−18% PEG 8000, 0.05 M potassium phosphate, pH 7.5 and 3% 2-methyl-2,4-pentanediol (MPD). The data for the apo-enzyme were collected on an in-house Rigaku rotating anode generator with Göbel mirrors and a Bruker AXS CCD detector Smart 6000 at 100 K. The crystals of the apoenzyme diffracted to a resolution of 2.1 Å and belonged to space group *C*2 with cell dimensions of a = 130.6 Å, b = 110.6 Å, c = 77.1 Å, and β = 116.2°. One crystal was soaked with 5 mM NAD^+ and 5 mM (*R*)-1-phenylethanol. Within the first hour, the crystal started to break apart. One piece was frozen immediately, and data of this crystal were collected at the synchrotron Swiss Light Source (Villingen, Switzerland). The crystal diffracted up to 2.4 Å resolution. Although the crystal had been grown under the same conditions as the crystal of the apo-protein, it showed a different, tetragonal space group with cell constants $a = b$ = 58.4 Å and c = 236.2 Å. Table 1 summarizes the data collection and processing statistics.

Structure Determination and Refinement. The structure of PED was solved by molecular replacement with the program CNX (*24*). As phasing model, we used the tetrameric β-oxoacyl-[acyl carrier protein] reductase of *E. coli* (PDB ID: 1I01) (*25*), which shows 33% sequence identity. With a restricted dataset between 15 and 4 Å, clear solutions for the rotation and translation search above noise level were obtained. The positioned tetramer was subjected to one round of simulated annealing by torsion-angle dynamics (*26*). An electron-density map was calculated with data to 2.1 Å resolution. Inspection of the map showed electron density of the true side chains in many cases, which were corrected with the program QUANTA (Accelrys, San Diego, CA). Several rounds of simulated annealing with Cartesian dynamics and manual rebuilding improved the model. At a later stage, simulated annealing was omitted, and the rebuilt models were subjected to positional refinement with bulk solvent correction as implemented in CNX. Water molecules and two sulfate ions were added. The refinement continued until no further improvement was achieved. The final model has proper stereochemistry and good R-values (Table 2). The structure of the tetragonal crystal form was solved by molecular replacement calculations using the model of the apo-enzyme as search molecule with all data to 2.4 Å resolution.

Table 1: Statistics of X-ray Data Collection

	apo structure	soaked crystal[a]
space group	C2	$P4_32_12$
resolution range (Å)	59.6−2.1 (2.18−2.1)[b]	22.4−2.4 (2.5−2.4)[b]
reflections	56048 (5409)[b]	16156 (1750)[a]
completeness (%)	98.2 (95.2)[b]	92.0 (86.8)[b]
R_{sym}	0.07 (0.216)[b]	0.073 (0.122)[b]
I/σ	5.9 (1.8)[b]	14.5 (11.34)[b]

[a] With NAD^+ and (*R*)-1-phenylethanol. [b] Values in parentheses indicate high-resolution shell.

Table 2: Structure Refinement Statistics

	apo enzyme	soaked crystal[a]
resolution (Å)	59.6−2.1	22.4−2.4
reflections (for R_{free})	56112 (4250)[b]	15349 (809)[b]
completeness (%)	97.6	90.5
R_{work}	0.171	0.180
R_{test}	0.210	0.260
Rms deviations from ideal stereochemistry		
bond lengths (Å)	0.004	0.006
bond angles (deg)	1.2	1.4
dihedrals (deg)	22.8	22.8
impropers (deg)	0.7	3.7
mean B-factor (Å^2)	16.5	33.5
Ramachandran plot		
most favored regions (%)	91.8	91.5
allowed regions)%)	8.2	8.5

[a] With NAD^+ and (*R*)-1-phenylethanol. [b] Values in parentheses indicate high-resolution shell.

Modeling of acetophenone in the active site was performed with the program QUANTA. The molecule was created with the 2D sketcher and converted to a 3D structure, and the geometries were optimized with the program built-in minimizer. The molecule was manually positioned in the active site. The distances between the reactive oxo-group and the respective atoms of the active site (OH of Tyr154, OH of Ser141) and the cofactor (C4 of the nicotinamide ring) were chosen to mimic the productive complex. Coordinates of the two structures have been deposited in the Protein Data Bank (apo-protein PDB ID 2EW8 and NAD^+ bound structure PDB ID 2EWM).

RESULTS

The Overall Structure. The structure of the apo-form of the enzyme was solved with a resolution at 2.1 Å. Its quality

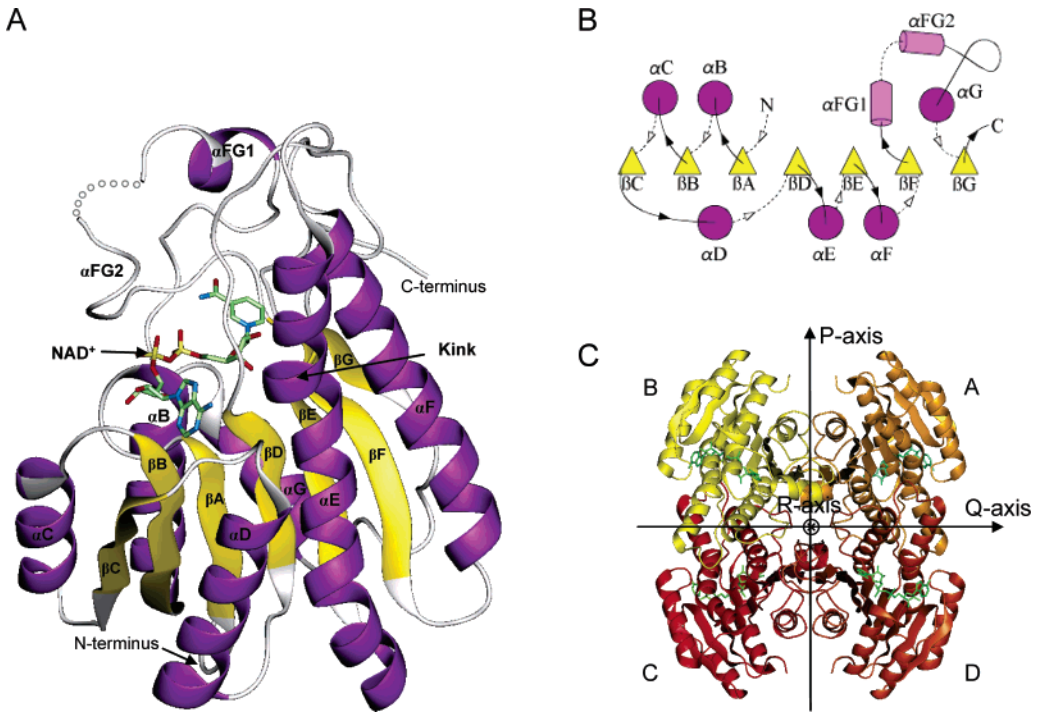

FIGURE 1: Overall structure of (*S*)-1-phenylethanol dehydrogenase from strain EbN1. (A) Structural overview of the monomer with α-helices in magenta and *β*-strands in yellow. The cofactor NAD^+ is shown. The disordered part of the substrate binding loop is indicated by a dotted line. The labeling convention with respect to the secondary structure elements is according to Ghosh et al. (*37*). (B) Schematic diagram of secondary structure elements and their consecutive arrangement. (C) Quaternary structure of the tetramer. Subunits A, B, C, and D are indicated by letters and colored light brown, yellow, red and orange, respectively. The arrows represent the symmetry axes, the R-axis is perpenticular of the paper.

is reflected by the low R-work and R-free values of 17.1 and 21.0%, respectively, with excellent stereochemical parameters (see Table 2). (*S*)-1-Phenylethanol dehydrogenase (PED) is a typical short-chain dehydrogenase/reductase with a classical Rossmann fold structure. It consists of a twisted parallel *β*-sheet composed of seven *β*-strands that is flanked on both sides by six helices as shown in Figure 1. The asymmetric unit contains one PED tetramer with a 222 symmetry, each subunit consisting of 230 amino acids (Figure 1). The model contains 600 water molecules with B-factors in the range of 4−60 $Å^2$. The substrate binding loops (amino acids 188−205) and the first two amino acids of all four subunits are disordered and not included in the model. The structures of the individual subunits of the tetramer are practically identical with only minor deviations at the crystal contact regions. In contrast to the similar structure of *β*-oxoacyl-[acyl carrier protein] reductase (FabG) (*27*), no crystallographically visible metal ions are present in PED.

The enzyme soaked with NAD^+ and the inhibitor (*R*)-1-phenylethanol formed a different crystal form containing two subunits in the asymmetric unit. The full tetramer is created by a crystallographic 2-fold axis. The amino acids forming contacts with the bound cofactor are shown in Figure 2. The structures of the subunits in the soaked crystal differ from those of the apo-form only in the substrate binding loop, while the rest of the molecule is virtually identical. The cofactor (NAD^+) binding sites in the two crystallographically independent subunits (A and B) are only partially occupied, as deduced from the relative weak electron density for the two cofactors. For this reason, the structure refinement was carried out with an assumed occupancy of 0.66. The electron

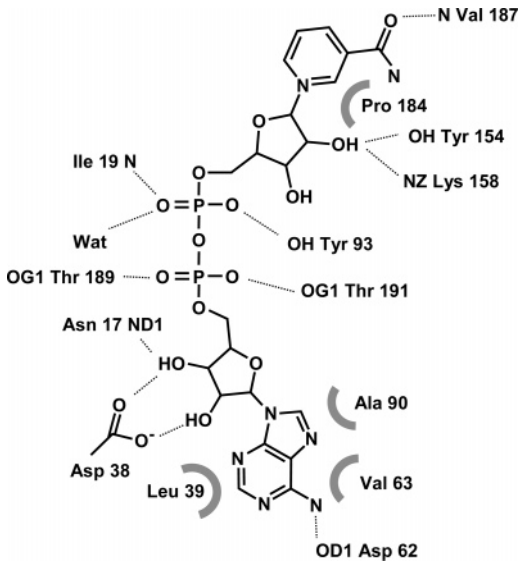

FIGURE 2: Schematic drawing of NAD^+−PED interactions.

density defining the adenine and adenine ribose moieties is significantly stronger than that of the nicotinamide ribose. The nicotinamide moiety itself is disordered. The binding of the NAD^+-cofactor apparently induces a partial ordering of the substrate binding loop. In contrast to the apo-form of the enzyme, electron density for amino acids 188−194 can be recognized in the soaked crystal, and these amino acids were added to the model. In subunit B, the remaining amino acids of the substrate-binding loop have also been modeled. Amino acids 201−208 form a short α-helix. The loop is stabilized by the side chain oxygens of threonines 189 and

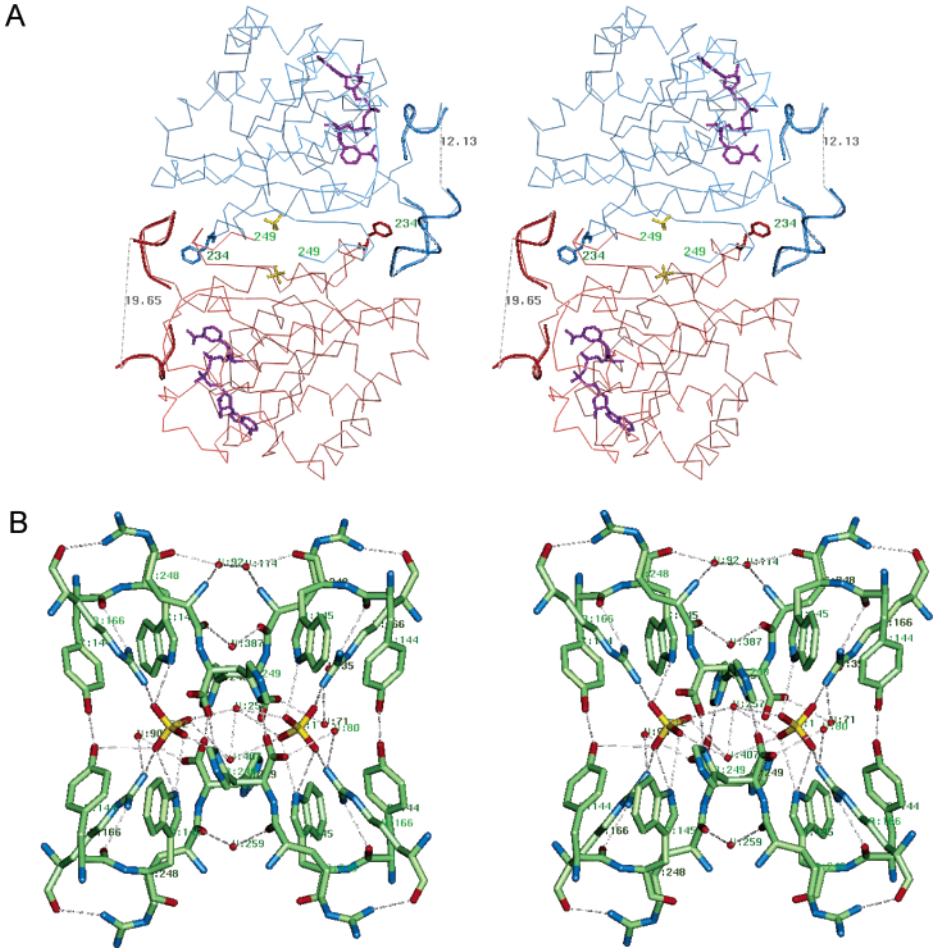

FIGURE 3: Stereo image of a substructure of two subunits of PED complexed with NAD^+. Highlighted are the substrate binding loops, NAD^+, SO_4^{2-}, the C-termini and Phe234, which protrudes into the substrate binding loop of the other subunit. The two subunits are connected via the P-axis interface (A). Stereo picture of the hydrogen bonding network around the C-termini of the four subunits of the tetramer (B).

191 forming hydrogen bonds to the phosphate of the adenine-half of NAD^+. Since the cofactors occupy the binding site only partially, the electron density is not very clear, as reflected in a high-temperature factor for this loop. Moreover, it is not clear from the electron density whether the inhibitor (*R*)-1-phenylethanol is bound. No electron density can unambiguously be assigned to the inhibitor in the active site, although an unstructured piece of electron density occupies part of the pocket. The NAD^+-induced ordering of the substrate binding loop has significant consequences for the active site. In particular, Leu186 moves out of the pocket where the substrate is expected to bind (Supplementary Figure 2, Supporting Information). Without this movement, the nicotinamide ring would be hindered from entering the active site in a productive conformation due to a steric conflict with the Cα atom of Leu186 (distance between Cα and NC4: 2.7Å). Concomitantly, the side chain of Ser185 is shifted, breaking a hydrogen bond with the side chain carbonyl oxygen of Asn215 in the apo-form and forming a new one with the side chain carbonyl oxygen of Gln209. At the same time the amido nitrogen atom of Asn215 becomes hydrogen-bonded to the main chain carbonyl group of Val242. This rearrangement also creates a pocket into which the phenyl ring of Phe234 of an adjacent subunit extends (Figure 3A). In most SDR sequences, Ser185 is replaced by a glycine (*28*), which is part of the so-called PG-motif and may be involved in cofactor interaction and affect reaction direction (*9*). The observed intercalation of Phe234 into the pocket formed by the substrate binding loop and concomitant residues near the C-terminus apparently also affects the prominent C-terminal hydrogen network and seems to be responsible for the cooperative properties of the enzyme (see Discussion).

The conformation of the NAD^+ and its binding mode is typical for the SDR family. The NAD^+ is in an extended conformation, and the adenine and nicotinamide rings are oriented approximately perpendicular to the planes of the respective riboses, resulting in an anti-conformation of the adenine ring and a syn-conformation of the nicotinamide ring. The distance of about 13.5 Å between C6 of the adenine and C2 of the nicotinamide lies within the distances reported by Benach et al. (*29*) for several other SDRs. There are 11 hydrogen bonds between the cofactor and the protein and one water-mediated hydrogen bond (Supplementary Figure 2, Supporting Information). The adenine ring fits into a hydrophobic cleft formed by Ala 90, Val63, and Leu39. The side chain of Asp38 forms hydrogen bonds with the two hydroxyl groups of the adenine ribose. The nicotinamide is positioned in the active site cleft with its Re-face toward a hydrophobic wall comprised of Pro184, Val187, Ile19, and Leu139. Pro184 is highly conserved in the classical SDRs, and also Ile19 and Leu139 belong to a conserved patch of

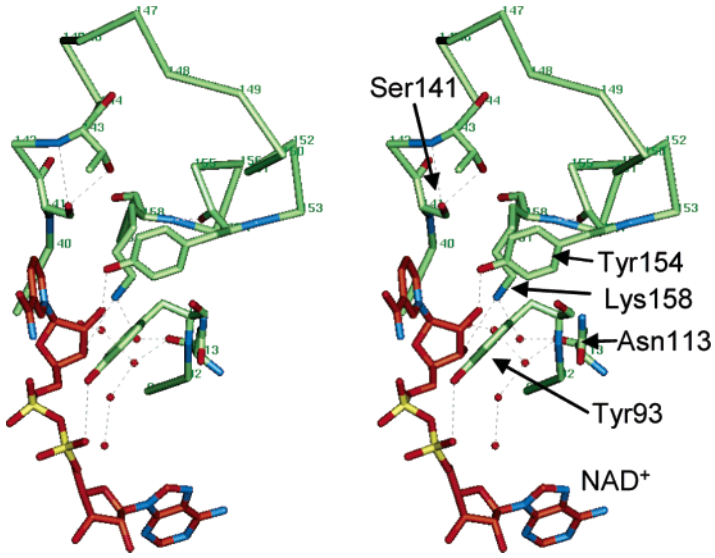

FIGURE 4: Active site with cofactor NAD^+. The conformation of the conserved amino acids Ser141, Tyr154, Lys158, and Asn113 relative to the bound NAD^+ and a chain of structurally conserved water molecules is shown. In addition, the Tyr93 protruding into the active site and probably conferring enantioselectivity is visible.

hydrophobic residues (*28*). The active-site residue Tyr154 points almost perpendicular to the Si-side of the nicotinamide ring, and the distance between the OH group and C6 of the nicotinamide ring is about 3.4 Å. Concomitantly, the OH group of Tyr154 is hydrogen bonded to O2 of the corresponding ribose, as is Lys158 of the active site.

The overall organization of the tetramer is very similar to that of FabG of *E. coli* (*27*). The tetramer exhibits two types of dimerization interfaces, the Q-axis related and the P-axis related interface (Figure 1C). The Q-axis interface is located between helices αE, αF and the same helices αE′ and αF′ of the neighboring monomers A and D, and B and C, respectively, the four helices forming a four helix bundle. The contact area of the Q-axis interface accounts for approximately 1670 $Å^2$ as calculated with the Protein−Protein Interaction Server (http://www.biochem.ucl.ac.uk/bsm/PP/server/). The majority of the interactions (64%) are classified as nonpolar, and 13 hydrogen bonds were identified. The second dimerization interface, the P-axis interface, is formed by strand *β*G, helix αG, and the C-terminus of the subunits. The contact area adds up to 1510 $Å^2$ with 52% nonpolar interactions, 11 hydrogen bond, and two salt bridges. The structure of the C-termini is particularly noteworthy: all four terminal histidine residues of the subunits come close together and are part of a widespread network of hydrogen bonds (Figure 3B). The interactions are highly symmetric because the center of the 222 point group symmetry of the tetramer is located in the center of the four histidines. The histidines of monomers A and B and those of monomers C and D, respectively, show a special hydrogen bonding pattern between one of the oxygen atoms of the carboxy-terminus and a nitrogen of the imidazol ring of the neighboring histidine (ND1). Moreover, two sulfate ions are bound in the vicinity, each of which is involved in bridging of two monomers, subunits A/D and B/C, respectively (Figure 3B). The hydrogen-bridged atoms of the PED subunits are the nitrogen of the indol ring of Trp145 (NE1) and a nitrogen of Arg166 (NH2). The two sulfate ions themselves are connected by two water molecules (nos. 491 and 492).

The side chains of the universally conserved active-site amino acids Tyr154, Lys158, and Ser141 are situated in the same positions in the apo-form and in the NAD^+-bound form of the enzyme (Figure 4). Thus, in contrast to FabG, no structural rearrangement is required to arrange these amino acids into a catalytically competent conformation. The cofactor-induced switch of Leu186 in the substrate-binding loop of PED alone seems to be responsible for binding of NAD^+ and will also allow binding of the substrate, suggesting that the enzyme sequentially binds first NAD^+ and then the substrate, as usual for SDRs. The fourth highly conserved active site residue Asn113 is part of helix αE at a kinked region, with its side chain carbonyl group hydrogen-bonded to the main chain amino group of Ile92 (OD1—N, ND2—O). The main chain carbonyl oxygen of Asn113 is part of an hydrogen bonding network, which serves as proton relay system (Figure 4) (*30*). Many of the water molecules contributing to this network are structurally conserved. The special arrangement of Asn113 leads to the observed kink in helix αE, a feature found in many SDR structures (*31*).

Modeling of Acetophenone into the Active Site. Figure 5 shows the modeling of acetophenone into the active site. The molecule was manually positioned in the same manner as described by Niefind et al. (*8*) for the (*R*)-specific alcohol dehydrogenase from *L. brevis*. The oxygen of the oxo-group was positioned within hydrogen bonding distance to the OH groups of Tyr154 (2.8 Å) and Ser141 (2.8 Å). The carbon atom of the oxo-group was placed in such a way that a hydride transfer would be reasonable from C4 of the nicotinamide ring (2.9 Å distance). With these geometric constraints and avoiding steric conflicts with the surrounding atoms, only one placement of acetophenone is possible in the active site, which will lead to generation of (*S*)-1-phenylethanol after reduction. Productive placement for obtaining the (*R*)-alcohol would require turning the acetophenone around the keto bond by 180°, leading to a steric clash with Tyr93. Interestingly, the active site of (*R*)-specific alcohol dehydrogenase from *L. brevis* shows a very similar amino acid arrangement, only in a mirror-inverted conformation. In this case, a different tyrosine (Tyr189) protruding

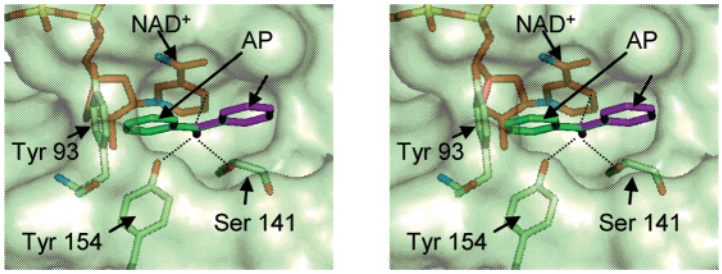

FIGURE 5: Stereo image of the modeling of acetophenone (AP) in the active site. The substrate is shown both in catalytically productive conformation (purple) and in a nonproductive conformation, which can be excluded because of steric hindrance with Tyr93 (green).

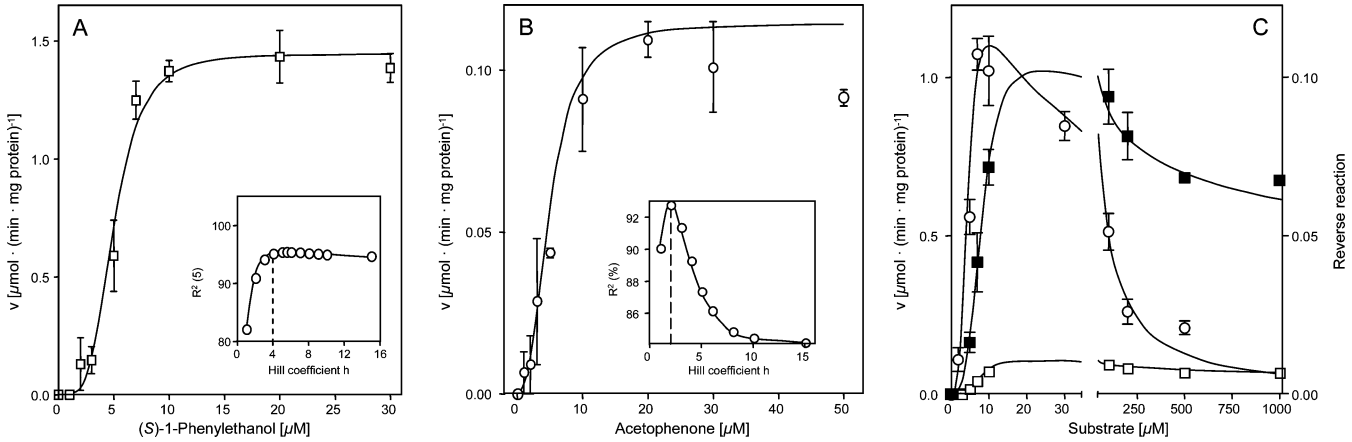

FIGURE 6: Steady-state kinetics of (*S*)-1-phenylethanol dehydrogenase. The forward (A) and the reverse reaction (B) of the enzyme, as measured in assays containing 0.5 mM NAD^+ or 0.5 mM NADH, respectively, have been analyzed and evaluated by curve fitting against the Hill equation. The insets show the effects of fitting the respective data with different fixed Hill coefficients in the range of 1−15 on the quality of the fit (R^2 values). The broken line in the inset of (A) indicates the beginning of a plateau of R^2 values reached at a Hill coefficient of 4.0; in case of (B) it indicates the optimum Hill coefficient of 2.0. (C) Substrate-inhibition of (*S*)-1-phenylethanol dehydrogenase of both forward (open circles) and reverse reaction (open squares). The data of the reverse reaction are additionally plotted in a 10-fold enlarged scale (filled squares; right ordinate). The curves were obtained by fitting the data to eq 3. The following parameters were obtained for the forward reaction: $V = 1.7$ µmol min^{-1} mg^{-1}; $K_{0.5} = 5.5$ µM; $h = 4.0$; $n = 0.74$; $K_{is} = 28$ µM, and for the reverse reaction: $V = 0.16$ µmol min^{-1} mg^{-1}; $K_{0.5} = 11.3$ µM; $h = 2.0$; $n = 0.37$; $K_{is} = 277$ mM.

into the active site would lead to a clash with acetophenone binding in an orientation leading to the (*S*)-enantiomer of the alcohol (*8*).

Molecular Mass of (S)-1-Phenylethanol Dehydrogenase. The composition of PED as a homotetramer of four 27 kDa-subunits is in apparent contrast to the previously determined native mass of the enzyme, which suggested a homodimeric structure (*13*). Therefore, we reanalyzed the molecular mass of the recombinant enzyme used for crystallization by two independent methods, gel filtration chromatography and Ferguson plot analysis of native polyacrylamide gels. Whereas the gel filtration experiments confirmed the earlier data, yielding an apparent mass of 59 kDa for (*S*)-1-phenylethanol dehydrogenase, the same batch of enzyme migrated in native gels with an apparent mass of 93 kDa, which is consistent with the tetrameric structure derived by X-ray crystallography (data not shown). Thus, PED appears to behave aberrantly on gel filtration chromatographic columns, possibly caused by retardation of the enzyme by interaction with the column material.

Cooperative Catalysis of (S)-1-Phenylethanol Oxidation and Acetophenone Reduction. Detailed analysis of the steady-state kinetics of PED in the forward and reverse directions showed that both NAD^+-dependent oxidation of (*S*)-1-phenylethanol as well as NADH-dependent reduction of acetophenone follow sigmoidal curves (Figure 6), suggesting positive cooperativity of both reaction directions. The measured data were directly fitted against the Hill equation:

$$v = V_{max} a^h (K_{0.5}{}^h + a^h)^{-1} \quad (1)$$

Nonlinear fits without constrained parameters yielded Hill coefficients (*h*) of 5.5 for the forward and 2.0 for the reverse reaction, using the data given in Figure 6 and a number of further data sets (excluding data obtained with inhibitory acetophenone concentrations of ≥30 µM). It is obvious that the Hill coefficient of a tetrameric enzyme should not exceed a value of 4.0 (the number of active sites), suggesting that the obtained coefficient of 5.5 is deceptive. Therefore, the experimental data were fitted separately against equations with fixed Hill coefficients ranging from 1 (noncooperative) to 15, and the correlation terms (R^2) of the obtained curve fits were plotted against the Hill coefficients (Figure 6A). This showed that the quality of fitting increased steadily up to a Hill coefficient of 4.0, but did not significantly improve further with increasing values of *h* (Figure 6A). Therefore, we used a Hill coefficient of 4.0, the theoretical maximum for a tetrameric enzyme, for the curve fit and for further calculations. After the fitting of the reverse reaction by the same procedure was tested, the Hill coefficient of 2.0 was clearly at an optimum (Figure 6B). A V_{max} value of 1.4 µmol min^{-1} (mg of protein)$^{-1}$ was determined for the forward reaction, whereas the reverse reaction showed a 12-fold lower V_{max} value (Figure 6). However, the $K_{0.5}$ values (substrate

concentrations yielding half-maximal activity) for the forward and reverse reactions were in a similar and rather low range (5.1 μM (*S*)-1-phenylethanol and 6.2 μM acetophenone; Figure 6). This suggests very high affinity of the enzyme toward its substrates in both directions and fits well with the very low K_m values observed for ethylbenzene dehydrogenase (<2 μM) (*13*) and acetophenone carboxylase (<5 μM; Jobst and Heider, unpublished), the preceding and following enzymes in the pathway of anaerobic ethylbenzene catabolism.

Substrate and Product Inhibition of (S)-1-Phenylethanol Dehydrogenase. The forward reaction of PED followed sigmoidal steady-state kinetics at substrate concentrations of <30 μM (Figure 6A) but higher concentrations of (*S*)-1-phenylethanol exerted strong substrate inhibition of the reaction. The reaction velocity was reduced to half of the observed maximum activity with 100 μM (*S*)-1-phenylethanol (Figure 6C). Because there are no established procedures for mathematical evaluation of substrate and product inhibition of highly cooperative enzymes, we tried to fit the data to rate equations derived from those describing inhibition of noncooperative enzymes, which were modified in their substrate concentration terms in analogy to the Hill equation. Substrate inhibition normally follows an uncompetitive kinetic scheme that is described by the following equation for noncooperative enzymes (*32*):

$$v = V_{max} a (K_m + a + a^2 K_{is}^{-1})^{-1} \quad (2)$$

with *a*: substrate concentration; K_{is}: substrate inhibition constant.

Considering the cooperativity of the enzyme with respect to its substrate, the terms for substrate concentration (*a*) and K_m ($K_{0.5}$, respectively) were taken to the power of *h* in analogy to the Hill equation, resulting in the following equation:

$$v = V_{max} a^h (K_{0.5}{}^h + a^h + a^{h+n} K_{is}^{-n})^{-1} \quad (3)$$

The exponent *n* of the inhibitory term was left undetermined rather than assigning it as 1.0 to avoid imposing too much bias on the curve fit.

Curve fitting of the data of the forward reaction with the unconstrained equation yielded a value of the Hill coefficient *h* of 4.2. Therefore, we constrained the value of *h* to 4.0 to obtain fits for the other parameters. The overall fit as shown in Figure 6C correlated very well with the measured data (R^2 = 94%). The calculated theoretical value of V_{max} of 1.7 μmol min^{-1} (mg of protein)$^{-1}$ is significantly higher than the maximum value obtained from curve fitting of the data from low substrate concentrations against the Hill equation (Figure 6A), indicating that (*S*)-1-phenylethanol may already have inhibitory effects in a range of 20−30 μM. In contrast, the calculated $K_{0.5}$ of 5.5 μM is only slightly higher than that obtained previously. The curve fitting procedure also yielded values of 0.74 for the empirical exponent *n* and 28 μM for the substrate inhibition constant K_{is}.

The reverse reaction was also sensitive to substrate inhibition, if more than 20 μM acetophenone were added to the test (Figure 6C). Substrate inhibition of the reverse reaction was much weaker than that of the forward reaction, and the reaction still operated at 75% of its maximum activity with 1 mM acetophenone (Figure 6C). Yet, because of the 10-fold lower activity of the enzyme for the reverse reaction, equal activities of the enzyme in both directions were only reached at about 1 mM substrate each (Figure 6C). The data were fitted to the modified rate equation for substrate inhibition introduced above (eq 3), yielding the following values for the kinetic parameters: V_{max} = 0.16 μmol min^{-1} (mg of protein)$^{-1}$, $K_{0.5}$ = 11.3 μmol, K_{is} = 277 μmol, *h* = 2.0, and *n* = 0.37. As seen for the forward reaction, it appears that the enzyme may already be inhibited at low acetophenone concentrations and therefore does not reach the potential maximum activity of acetophenone reduction.

Moreover, forward and reverse reactions were also strongly inhibited by the respective reaction products. Product inhibition followed hyperbolic curves with increasing half-inhibitory inhibitor concentrations at several tested substrate concentrations, with the reverse reaction being apparently even more susceptible to product inhibition than the forward reaction (Supplementary Figure 3, Supporting Information).

Non-Cooperative NAD$^+$ Binding and Reaction Mechanism. Whereas PED revealed strong cooperativity toward (*S*)-1-phenylethanol, the second substrate of the enzyme, the NAD$^+$ cofactor, is apparently not bound in a cooperative manner. Steady-state kinetics of the enzyme with varying NAD$^+$ concentrations always followed normal Michaelis−Menten curves (Hill coefficients of 1.0) at different constant (*S*)-1-phenylethanol concentrations in the nonsaturating, the saturating, and the inhibitory range (data not shown). NAD$^+$ also did not exert substrate inhibition at concentrations up to 500 μM (data not shown).

Using a series of assays with varied (*S*)-1-phenylethanol concentrations at different constant NAD$^+$ concentrations, we tried to get evidence on the catalytic parameters of NAD$^+$ binding and on the reaction type of the enzyme (Figure 7A). Curve fitting of all data sets revealed that the reactions followed sigmoidal kinetics. Moreover, all curves except one fitted to equations with a constant Hill coefficient of 4.0. The exception was recorded for the data set with the lowest NAD$^+$ concentration (2 μM), which yielded a Hill coefficient of 2.3 during curve fitting. Thus, this might be explained by incomplete occupation of the active sites by NAD$^+$, which may affect subsequent substrate binding.

The different apparent maximum rates V_{app} at different NAD$^+$ concentrations have been recorded and evaluated using the equation for noncooperative enzymes (eq 4) (*32*).

$$V_{app} = V[NAD^+](K_{m(NAD^+)} + [NAD^+])^{-1} \quad (4)$$

A secondary Lineweaver−Burk-like plot of the inverse values of the NAD$^+$ concentrations versus the V_{app} values obtained from curve fitting indeed yielded the expected straight line (Figure 7B). Moreover, a reasonable K_m value for NAD$^+$ of 4.7 μM was extrapolated by this approach. Because the NAD$^+$ concentration in the routine assay (0.5 mM) is >100-fold higher than this K_m value, we can safely assume that the (apparent) $K_{0.5}$ values for (*S*)-1-phenylethanol obtained in the former experiments are good approximations of the true values.

Conversion of the Hill equation for PED to a form analogous to the Lineweaver−Burk plot yields eq 5:

$$v^{-1} = K_{0.5}{}^4 V_{max}{}^{-1} a^{-4} + V_{max}{}^{-1} \quad (5)$$

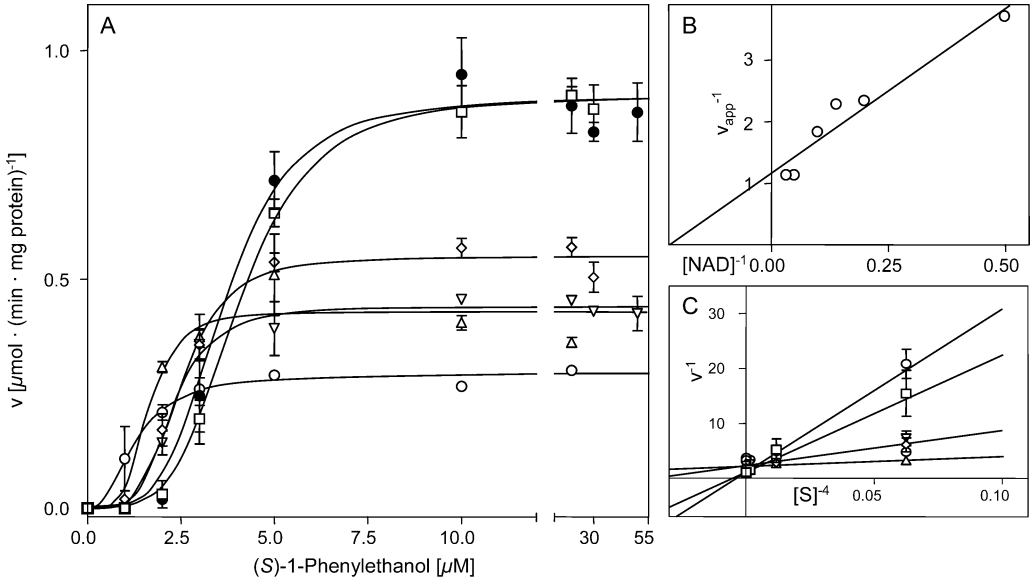

FIGURE 7: Reaction mechanism of (*S*)-1-phenylethanol dehydrogenase. (A) Kinetics of (*S*)-1-phenylethanol oxidation at different concentrations of NAD^+: 2 μM (circles); 5 μM (triangles); 7 μM (inverted triangles); 10 μM (diamonds); 20 μM (squares); 30 μM (filled circles). Except for the data set for the lowest substrate concentrations, all curves were fitted to the Hill equation with $h = 4.0$. (B) Secondary plot of NAD^+ concentrations versus the respective apparent V_{max} values from Figure 7A. (C) Lineweaver−Burk-like representation of the data from (A) (excluding the data obtained with 2 μM NAD^+ that did not fit to a Hill coefficient of 4.0).

Thus, straight lines are expected if a^{-4} is plotted against v^{-1}. Converting the data of Figure 7A into this form yields straight lines that cross at one point (Figure 7C). In analogy to noncooperative enzymes, this may be taken as indication that the reaction proceeds via a ternary complex of the enzyme and the two substrates, as expected for NAD^+-dependent dehydrogenases. To avoid distortion of the data, the apparent $K_{0.5}$ and V_{max} values obtained from the nonlinear curve fits were used to draw the lines of the linear plot.

Inhibitory Effects of (R)-1-Phenylethanol. It had been observed previously that the (*R*)-enantiomer of 1-phenylethanol inhibits PED (*13*). Therefore, the influence of this inhibitor on enzyme kinetics has been further studied. First, the effects of mixing the two enantiomers in different ratios on the kinetics of 1-phenylethanol oxidation have been determined. Increasing concentrations of (*R*)-1-phenylethanol, mixed with (*S*)-1-phenylethanol, resulted in steadily decreasing V_{max} values, decreasing Hill coefficients, and increasing $K_{0.5}$ values (Supplementary Figure 4, Supporting Information). However, all curves showed clear cooperativity. The clear inhibitory effects exerted by the "wrong" enantiomer on PED activity were investigated in more detail by analyzing steady-state kinetics in the presence of increasing concentrations of (*R*)-1-phenylethanol (Figure 8). The (*R*)-enantiomer affected the catalytic properties of the enzyme already at very low concentrations. The most pronounced effect of the inhibitor is a very sharp drop in the Hill coefficient of the reaction, which is approaching 1.0 at inhibitor concentrations of >20 μM (Figure 8B). No general trend is seen in the courses of the $K_{0.5}$ and V_{max} values, probably because the dominant effect of the inhibitor on cooperativity masks the effects on other parameters (Figure 8B). However, when concentrations of >70 μM (*R*)-1-phenylethanol were added, the reaction was strongly inhibited, and V_{max} values dropped to a similar extent as observed for substrate inhibition by (*S*)-1-phenylethanol (Figure 8). Finally, the effects of (*R*)-1-phenylethanol on acetophenone-reduction were analyzed. Addition of 50 μM of the inhibitor to an assay started with 25 μM acetophenone led to a drop of enzyme activity by 50%. However, (*R*)-1-phenylethanol did not completely block acetophenone reduction activity, which remained at approximately 25% of the noninhibited rate even in the presence of high inhibitor concentrations (Supplementary Figure 5, Supporting Information).

DISCUSSION

Kinetic Behavior of PED. Price et al. (*27*) solved the structure of β-oxoacyl-[acyl carrier protein] reductase (FabG) and described a conformational rearrangement of parts of the protein structure upon binding of the NADH cofactor. They associated this conformational switch with the observed negative cooperativity of the enzyme with respect to NADH. Because the structure of the apo-form of FabG was similar enough to that of PED to serve as model for solving the structure, we initially expected a similar mechanism for PED. To our surprise, however, detailed kinetic studies with PED showed clearly that it behaves differently from FabG. The enzyme proved to be positively cooperative with high Hill coefficients with respect to the alcohol and ketone substrates but noncooperative with respect to NAD^+. Similar positive cooperativity toward the substrates and noncooperative behavior toward the $NAD(P)^+$ cofactor has previously been observed for other members of the SDR enzyme family (*33*, *34*), although these enzymes are not very closely related to PED based on sequence similarity. Moreover, PED was substrate- and product-inhibited for both (*S*)-1-phenylethanol oxidation and acetophenone reduction. Such strong regulation is quite unusual for an enzyme like PED that does not catalyze an irreversible step in the catabolic pathway. The regulation pattern of PED apparently causes the enzyme to be optimally active only when low concentrations of substrate and product are present in the cytosol. This fits well with the low K_m values of all known enzymes of the ethylbenzene catabolic pathway. If (*S*)-1-phenylethanol and acetophenone

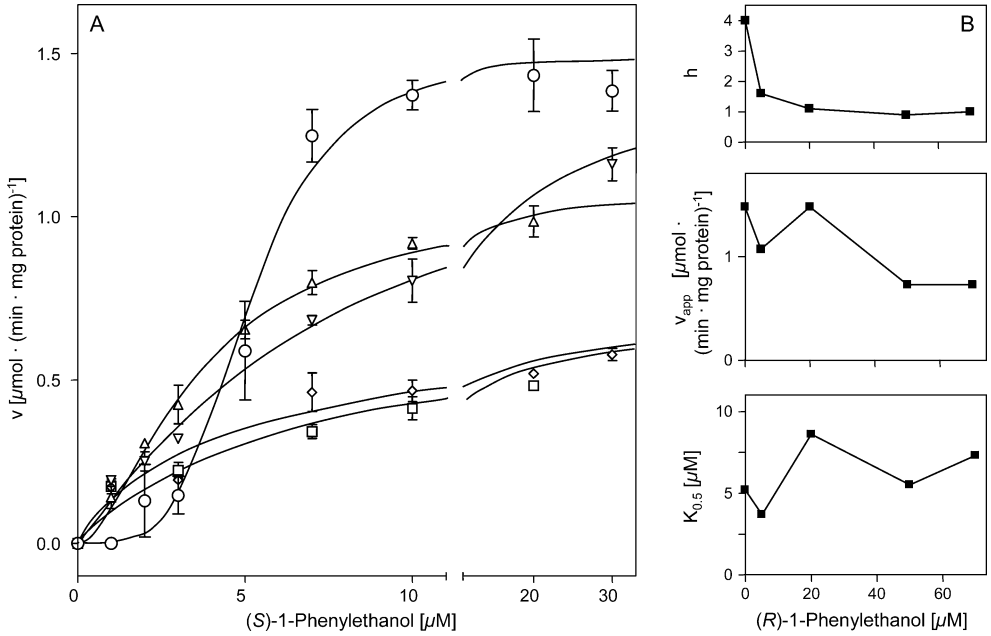

FIGURE 8: Inhibitory effects of (*R*)-1-phenylethanol. (A) Assays with (*S*)-1-phenylethanol in the presence of varying concentrations of the (*R*)-enantiomer: none (circles); 5 μM (triangles); 20 μM (inverted triangles); 50 μM (diamonds); 70 μM (squares). (*S*)-1-Phenylethanol concentrations in the respective tests are indicated on the *x*-axis. (B) Effects of added (*R*)-1-phenylethanol concentrations on the kinetic parameters of (*S*)-1-phenylethanol dehydrogenase.

concentrations exceed these low values, they inhibit both alcohol oxidation and ketone reduction activity of the enzyme. However, it might be noteworthy that acetophenone reduction is much less severely substrate-inhibited than (*S*)-1-phenylethanol oxidation. Therefore, at elevated acetophenone concentrations, a shift of equilibrium of PED toward reduction of the ketone might be a measure to cope with toxic effects of acetophenone. PED is exclusively present in ethylbenzene-grown cells (*35*) (Kniemeyer and Heider, unpublished results), and the observed regulatory pattern would somewhat restrict the metabolic flux from ethylbenzene to acetophenone. Moreover, acetophenone may also be detoxified by reduction to (*R*)-1-phenylethanol by an (*R*)-specific isoenzyme. At least one (*R*)-1-phenylethanol dehydrogenase and another PED isoenzyme appear to be present in ethylbenzene-grown cells. Therefore, accumulation of (*R*)-1-phenylethanol appears to take part in the regulation of PED, again acting more restrictively on alcohol oxidation than on ketone reduction. A scheme of the observed regulatory effects of the metabolites is shown in Figure 9. The presence of other (*S*)- and (*R*)-1-phenylethanol dehydrogenases, probably with a different type of regulation, also provides a possibility to rescue the catabolic pathway, if PED activity is shut down by accumulation of too much substrate.

Active Site Structure and Enantiomer Specificity. The different kinetic behavior of PED, compared to FabG, is corroborated by the observed structures of the apo-form of PED and the NAD^+-containing enzyme, which did not show the significant structural changes described for FabG (*27*). In contrast to FabG, the conformation of the active site of PED appears to be unchanged between the apo-form and the enzyme containing NAD^+. In both forms, the universally conserved active site residues of short-chain dehydrogenases, Ser141, Tyr154, Lys158 and Asn113, together with the OH groups of the nicotinamide ribose and a chain of bound water molecules, form a network of hydrogen bonds that is also

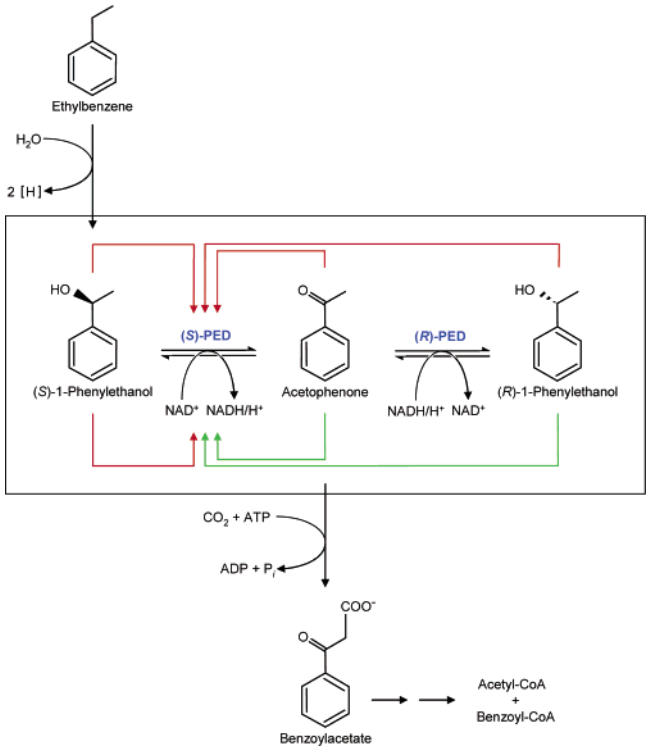

FIGURE 9: Summary of regulatory effects on PED. Inhibitory effects affecting the forward-reaction are shown above, while the regulatory effects on the reverse reaction are indicated below the reaction arrow. Strong inhibition by the respective compounds is depicted by red arrows, and weak inhibition are depicted by green arrows.

found in other known structures of these enzymes. The conformation of these residues is fully consistent with the mechanism presented for FabG (*27*), which involves binding and activation of acetophenone via hydrogen bonds between the oxo-group and the OH groups of Ser141 and Tyr154. Acetophenone is then reduced via a concerted transfer of a

hydride from NADH and a proton from Tyr154 to the oxo-group. The deprotonated Tyr154 would then regain its proton from the solvent via a proton relay system involving Lys158, the ribose hydroxyls, and the chain of bound water molecules. A speciality of PED appears to be the side chain of Tyr93 that protrudes into the active site and appears to be responsible for the enantio-specificity of the enzyme. This is especially evident from comparison of the PED structure with that of (*R*)-specific alcohol dehydrogenase from *L. brevis*, which has also an extra protruding tyrosine (Tyr189) in the active site, albeit from a completely different region of the enzyme and arranged in mirror-imaged conformation (*8*). It should be noted that the statements on enantiomer selectivity are not based on an actual structure of substrate-bound PED. However, the critical residue Tyr93 is not part of the flexible substrate loop and therefore should not change its position very much upon substrate binding.

Structural Basis of NAD$^+$ Specificity. PED does not contain any of the crucial amino acids required for specific binding of NADP$^+$ in FabG and other NADP$^+$-specific enzymes of the SDR family (e.g., Ser14, Arg15, and Thr37 of FabG, all hydrogen-bonding to the 2′-adenine-ribose phosphate of NADP$^+$) (*27*). Instead, it contains an aspartate (Asp41) conserved in NAD$^+$-dependent enzymes of the SDR family that binds to the two OH groups of the adenine-ribose of the NAD$^+$ cofactor. Together with the steric effects of the adjacent Leu42, this discriminates against binding of NADP$^+$, as observed in the NAD$^+$-dependent 3-α-hydroxysteroid-dehydrogenase of *Comamonas testosteroni* (*36*).

Conformational Change and Cooperativity. The only large change induced in the NAD$^+$-bound form of PED involves the substrate-binding loop of PED, which shifts from a crystallographically disordered to a more ordered form and apparently allows NAD$^+$ and substrate binding only in the latter form. We propose that this structural rearrangement may also be correlated with the shifting between the inactive and the active forms of PED during cooperative catalysis. We suggest a three-step mechanism of catalysis. First, NAD$^+$ binds to the enzyme, partially ordering the substrate binding loop, including the switch of Leu186 that allows subsequent binding of substrate. Second, binding of the substrate probably leads to further rearranging and closing the substrate binding loop for catalysis. Third, this final repositioning of the substrate binding loop is transmitted to the other active sites. This transmittance is probably mediated by Phe234 that reaches out from the neighboring subunit and is sandwiched between the substrate binding loop and the last turn preceding the C-terminus of each subunit (Figure 5). Movement of Phe234 is probably transmitted to the other active sites via the special arrangement of the C-terminal amino acids and bridging sulfates, a special structural feature of PED that is lacking in FabG. Interestingly, the dimeric 3α-hydroxysteroid dehydrogenase/carbonyl reductase from *C. testosteroni* shows a similar C-terminal structural arrangement that may be involved in cooperative behavior as well, as speculated by Grimm et al. (*36*). The data show that despite the strong overall similarity of PED to other known enzymes of the SDR family, there are profound differences in the mechanisms of catalysis and cooperativity, which are apparently caused by subtle changes in the structures of these enzymes.

ACKNOWLEDGMENT

M. Kube (Berlin) is acknowledged for providing the *ped* clone.

SUPPORTING INFORMATION AVAILABLE

Purification of (*S*)-specific 1-phenylethanol dehydrogenase (PED) (Supplementary Table 1 and Figure 1); a close-up view of the NAD$^+$-binding pocket and the flexible loop with Leu186 (Supplementary Figure 2); inhibition of forward and reverse reactions of PED by the respective products (acetophenone and (*S*)-1-phenylethanol) (Supplementary Figure 3); inhibition of PED by a mixture of the 1-phenylethanol enantiomers (Supplementary Figure 4); inhibition of the reverse reaction of PED by (*R*)-1-phenylethanol (Supplementary Figure 5). This material is available free of charge via the Internet at http://pubs.acs.org.

REFERENCES

1. Kroutil, W., Mang, H., Edegger, K., and Faber, K. (2004) Recent advances in the biocatalytic reduction of ketones and oxidation of *sec*-alcohols, *Curr. Opin. Chem. Biol. 8*, 120−126.
2. Faber, K. (2004) *Biotransformations in Organic Chemistry*, Springer-Verlag, Berlin.
3. Hummel, W. (1997) New alcohol dehydrogenases for the synthesis of chiral compounds, *Adv. Biochem. Eng. Biotechnol. 58*, 145−184.
4. Hummel, W. (1999) Large-scale applications of NAD(P)-dependent oxidoreductases: recent developments, *Trends Biotechnol. 17*, 487−492.
5. Jörnvall, H., Persson, M., and Jeffery, J. (1981) Alcohol and polyol dehydrogenases are both divided into two protein types, and structural properties cross-relate the different enzyme activities within each type, *Proc. Natl. Acad. Sci. U.S.A. 78*, 4226−4230.
6. Jörnvall, H., Höög, J.-O., and Persson, B. (1999) SDR and MDR: completed genome sequences show these protein families to be large, of old origin, and of complex nature, *FEBS Lett. 445*, 261−264.
7. Abokitse, K., and Hummel, W. (2003) Cloning, sequence analysis, and heterologous expression of the gene encoding a (*S*)-specific alcohol dehydrogenase from *Rhodococcus erythropolis* DSM 43297, *Appl. Microbiol. Biotechnol. 62*, 380−386.
8. Niefind, K., Müller, J., Riebel, B., Hummel, W., and Schomburg, D. (2003) The crystal structure of *R*-specific alcohol dehydrogenase from *Lactobacillus brevis* suggests the structural basis of its metal dependency, *J. Mol. Biol. 327*, 317−328.
9. Oppermann, U., Filling, C., Hult, M., Shafqat, N., Wu, X., Lindh, M., Shafqat, J., Nordling, E., Kallberg, Y., Persson, B., and Jörnvall, H. (2003) Short-chain dehydrogenases/reductases (SDR): the 2002 update, *Chem.-Biol. Interact. 143*−*144*, 247−253.
10. Cripps, R. E., Trudgill, P. W., and Whateley, J. G. (1978) The metabolism of 1-phenylethanol and acetophenone by *Nocardia* T5 and an *Arthrobacter* species, *Eur. J. Biochem. 86*, 175−186.
11. Itoh, N., Morihama, R., Wang, J., Okada, K., and Mizuguchi, N. (1997) Purification and characterization of phenylacetaldehyde reductase from a styrene-assimilating *Corynebacterium* strain, ST-10, *Appl. Environ. Microbiol. 63*, 3783−3788.
12. Peters, J., Minuth, T., and Kula, M. R. (1993) A novel NADH-dependent carbonyl reductase with an extremely broad substrate range from *Candida parapsilosis*: purification and characterization, *Enzyme Microb. Technol. 15*, 950−958.
13. Kniemeyer, O., and Heider, J. (2001) (*S*)-1-phenylethanol dehydrogenase of *Azoarcus* sp. strain EbN1, an enzyme of anaerobic ethylbenzene catabolism, *Arch. Microbiol. 176*, 129−135.
14. Rabus, R., Kube, M., Beck, A., Widdel, F., and Reinhardt, R. (2002) Genes involved in the anaerobic degradation of ethylbenzene in a denitrifying bacterium, strain EbN1, *Arch. Microbiol. 178*, 506−516.
15. Kniemeyer, O., and Heider, J. (2001) Ethylbenzene dehydrogenase, a novel hydrocarbon-oxidizing molybdenum/iron−sulfur/heme enzyme, *J. Biol. Chem. 276*, 21381−21386.

16. Rabus, R., and Widdel, F. (1995) Anaerobic degradation of ethylbenzene and other aromatic hydrocarbons by new denitrifying bacteria, *Arch. Microbiol. 163*, 96−103.
17. Heider, J., Spormann, A. M., Beller, H. R., and Widdel, F. (1999) Anaerobic bacterial metabolism of hydrocarbons, *FEMS Microbiol. Rev. 22*, 459−473.
18. Rabus, R. (2005) Biodegradation of hydrocarbons under anoxic conditions, in *Petroleum Microbiology* (Ollivier, B., and Magot, M., Eds.) pp 277−299, ASM-Press, Washington.
19. Rabus, R., Kube, M., Heider, J., Beck, A., Heitmann, K., Widdel, F., and Reinhardt, R. (2005) The genome sequence of an anaerobic aromatic-degrading denitrifying bacterium, strain EbN1, *Arch. Microbiol. 183*, 27−36.
20. Stumpp, T., Wilms, B., and Altenbuchner, J. (2000) Ein neues, L-Rhamnose-induzierbares Expressionssystem für *Escherichia coli*, *Biospektrum 6*, 33−36.
21. Korz, D. J., Rinas, U., Hellmuth, K., Sanders, E. A., and Deckwer, W. D. (1995) Simple fed-batch technique for high cell density cultivation of *Escherichia coli*, *J. Biotechnol. 39*, 59−65.
22. Sambrook, J., Fritsch, E. F., and Maniatis, T. (1989) *Molecular Cloning: A Laboratory Manual*, 2nd ed., Cold Spring Harbor Laboratory Press, Cold Spring Harbor, NY.
23. Coligan, J. E., Dunn, B. M., Ploegh, H. E., Speicher, D. W., Wingfield, P. T. (2004) *Current Protocols in Protein Science*, John Wiley & Sons, New York, NY.
24. Brunger, A. T., Adams, P. D., Clore, G. M., DeLano, W. L., Gros, P., Grosse-Kunstleve, R. W., Jiang, J. S., Kuszewski, J., Nilges, M., Pannu, N. S., Read, R. J., Rice, L. M., Simonson, T., and Warren, G. L. (1998) Crystallography & NMR system: a new software suite for macromolecular structure determination, *Acta Crystallogr. D: Biol. Crystallogr. 54*, 905−921.
25. Price, A. C., Zhang, Y.-M., Rock, C. O., and White, S. W. (2001) Structure of β-ketoacyl-[acyl carrier protein] reductase from *Escherichia coli*: negative cooperativity and its structural basis, *Biochemistry 40*, 12772−12781.
26. Brunger, A. T. (1991) Simulated annealing in crystallography, *Annu. Rev. Phys. Chem. 42*, 197−223.
27. Price, A. C., Zhang, Y.-M., Rock, C. O., and White, S. W. (2004) Cofactor-induced conformational rearrangements establish a catalytically competent active site and a proton relay conduit in FabG, *Structure 12*, 417−428.
28. Kallberg, Y., Oppermann, U., Jörnvall, H., and Persson, B. (2002) Short-chain dehydrogenases/reductases (SDRs). Coenzyme-based functional assignments in completed genomes, *Eur. J. Biochem. 269*, 4409−4417.
29. Benach, J., Atrian, S., Gonzàlez-Duarte, R., and Ladenstein, R. (1999) The catalytic reaction and inhibition mechanism of *Drosophila* alcohol dehydrogenase: observation of an enzyme-bound NAD-ketone adduct at 1.4 Å resolution by X-ray crystallography, *J. Mol. Biol. 289*, 335−355.
30. Filling, C., Berndt, K. D., Benach, J., Knapp, S., Prozorovski, T., Nordling, E., Ladenstein, R., Jörnvall, H., and Oppermann, U. (2002) Critical residues for structure and catalysis in short-chain dehydrogenases/reductases, *J. Biol. Chem. 277*, 25677−25684.
31. Yamamoto, K., Kurisu, G., Kusunoki, M., Tabata, S., Urabe, I., and Osaki, S. (2001) Crystal structure of glucose dehydrogenase from *Bacillus megaterium* IWG3 at 1.7 Å resolution, *J. Biochem. (Tokyo) 129*, 303−312.
32. Cornish-Bowden, A. (2004) *Fundamentals of Enzyme Kinetics*, 3rd ed., Portland Press, London.
33. Chai, X., Zhai, Y., and Napoli, J. L. (1997) cDNA cloning and characterization of a *cis*-retinol/3α-hydroxysterol short-chain dehydrogenase, *J. Biol. Chem. 272*, 33125−33131.
34. Su, J., Chai, X., Kahn, B., and Napoli, J. L. (1998) cDNA cloning, tissue distribution, and substrate characteristics of a *cis*-retinol/3α-hydroxysterol short-chain dehydrogenase isozyme, *J. Biol. Chem. 273*, 17910−17916.
35. Kühner, S., Wöhlbrandt, L., Hufnagel, P., Fritz, I., Hultschig, C., Kube, M., Reinhardt, R., and Rabus, R. (2005) Substrate-dependent regulation of anaerobic ethylbenzene and toluene metabolism in a denitrifying bacterium, strain EbN1, *J. Bacteriol. 187*, 1493−1503.
36. Grimm, C., Maser, E., Mobus, E., Klebe, G., Reuter, K., and Ficner, R. (2000) The crystal structure of 3α-hydroxysteroid dehydrogenase/carbonyl reductase from *Comamonas testosteroni* shows a novel oligomerization pattern within the short-chain dehydrogenase/reductase family, *J. Biol. Chem. 275*, 41333−41339.
37. Ghosh, D., Weeks, C. M., Grochulski, P., Duax, W. L., Erman, M., Rimsay, R. L., and Orr, J. C. (1991) Three-dimensional structure of holo 3α, 20β-hydroxysteroid dehydrogenase: A member of a short-chain dehydrogenase family, *Proc. Natl. Acad. Sci. U.S.A. 88*, 10064−10068.

BI051596B